Photodegradation of Triclosan on the Kaolinite Surface: Kinetic, Mechanistic, and Molecular Modeling Approach

Cyril Le Fur, Florent Goujon, Pascal Wong Wah Chung, Patrice Malfreyt, Mohamed Sarakha

ACS OMEGA

http://pubs.acs.org/journal/acsodf
Article

Photodegradation of Triclosan on the Kaolinite Surface: Kinetic, Mechanistic, and Molecular Modeling Approach

Cyril Le Fur, Florent Goujon, Pascal Wong Wah Chung, Patrice Malfreyt, and Mohamed Sarakha*

Cite This: ACS Omega 2023, 8, 38916−38925
Read Online

ACCESS | Metrics & More | Article Recommendations | Supporting Information

ABSTRACT: The photodegradation of triclosan (TCS) was investigated on the kaolinite surface. The quantum yield was evaluated, and the photoproducts were identified by HPLC/MS (LC/Q-TOF), showing that the phototransformation is completely different from that reported in aqueous solutions. In particular, the formation of dioxin derivatives was fostered and occurred with a higher efficiency when compared to aqueous solutions. This suggests that TCS has specific interactions with the clay that clearly modifies its photochemical behavior. Moreover, it has also been shown that higher concentrations of TCS, namely, higher than 1.0 μmol g^{-1} of kaolinite, lead to a significant decrease of the photodegradation rate constant and enhance the formation yield of dimer-type photoproducts. This suggests that the distribution of TCS is clearly not homogeneous at the clay surface and the formation of aggregates is more likely occurring. To get a better insight into this specific interaction, a molecular dynamic modeling of TCS adsorption at the surface of kaolinite was carried out. This clearly shows that when equilibrium is reached, TCS binds to the kaolinite surface by hydrogen bonds involving the phenol function of TCS and the hydroxyl groups of the kaolinite surface. Such behavior confers a particular conformation to the adsorbed TCS that is different from that obtained in water and which could be a key step to partially explain the specific photochemical reactivity in both media. In addition, several TCS molecules appear to interact with each other through the π-stacking (aromatic stacking) process while retaining this hydrogen bond with the kaolinite surface. This is clearly in favor of cluster formation on the clay surface and promotes dimer-type photoproducts.

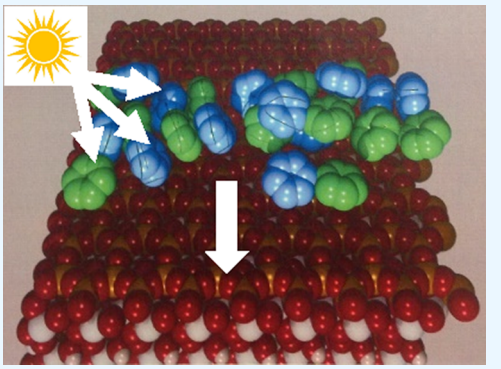

INTRODUCTION

Triclosan (TCS) is an antimicrobial compound that has been widely used in personal care products such as toothpaste, household products, body wash, soap, fabrics, as well as plastics. It is added to these products in order to mainly prevent bacterial development. It is known to disrupt the bacterial cell membrane leading certainly to its death ([1,2] and references therein). Thus, TCS is considered a kind of pharmaceutical and personal care products (PPCPs). It should be pointed out that this compound is linked to the development of antibiotic resistance bacteria as well as high perturbation of aquatic ecosystems when it enters natural waters.[3−10] The primary pathway for sewage to enter into the environment is the release of cosmetic products and detergents into wastewater during normal use. Although it is chemically stable in water, TCS is subject to photodegradation and biodegradation, which are effective in the aqueous phase. Indeed, its half-life time has been estimated at less than an hour under natural sunlight.[8−10] The photodegradation of TCS leads to the formation of a variety of byproducts, among them 2,4-dichlorophenol, 2,8-dichlorodibenzo-p-dioxin, and 2,4,8-trichlorodibenzo-p-dioxin.[11−16] The latter products are, of course, known to be more toxic and persistent than the parent compound and may naturally present an evident risk to the environment and human health.

When TCS is released into soil or sediment, it may be involved in various processes, such as adsorption to soil particles, degradation by microorganisms, or leaching into groundwater. The fate and behavior of TCS in soil and/or sediment depend on several factors, including soil characteristics, soil components, microbial activity, and environmental conditions in term of temperature, humidity, and solar light.[17−20] As in aqueous compartments, TCS can also present negative effects on soil such as inhibiting certain bacteria.[21] One of the important and possible pathways for the degradation of TCS at the surface of soils or clays as a model solid support is via photochemical reactions. When compared to the photochemistry in aqueous solutions,[11,22−25] the photochemical reactivity on soil may show several

Received: May 5, 2023
Accepted: September 22, 2023
Published: October 9, 2023

https://doi.org/10.1021/acsomega.3c03101
ACS Omega 2023, 8, 38916−38925

differences: (i) the adsorption of an organic molecule on a clay can greatly modify its absorption spectrum, leading to an increase of the overlap between the absorption spectrum of the compound and the emission spectrum of the sun, which will then enhance its photodegradation,[26,27] (ii) the photodegradation quantum yield of organic molecules as well as the photoproducts observed is very different from what is observed in water. The mechanism of photodegradation is therefore different at the surface of such support,[26−28] and (iii) the photosensitized and/or photoinduced degradation may be obtained through the formation of reactive species by excitation of organic matter such as humic substances[29−31] or through the generation of hydroxyl radicals from the clay components of the soil.[27,32] Moreover, the photochemistry of TCS may appear complex at the surface of soil and can be influenced by a variety of factors: soil components, light intensity, temperature, initial concentration, etc. Despite the very small thickness at which photodegradation can occur, understanding the photochemical behavior at the soil surface is a challenging topic, but it is really important for predicting the fate and effect of TCS on the environment in order to eventually develop strategies to minimize its potential impacts.

The present work concerns the photodegradation of TCS at the surface of kaolinite. Although a soil is a complex medium that is not exclusively composed of clay, kaolinite will be used here as a simplified soil model, as a first step toward understanding the processes involved in soil. Moreover, to better understand the process of adsorption of TCS at the kaolinite surface, which more likely affects the nature of the generated products, molecular dynamics simulations were undertaken.

EXPERIMENTAL SECTION

Chemical and Reagents. 5-Chloro-2-(2,4-dichlorophenoxy)phenol or TCS with the highest purity (99.0%) was purchased from Dr. Ehrenstorfer GmbH. It should be noted that, under our experimental conditions, dark controls tests showed that no degradation occurred under the preparation procedures. Methanol and acetonitrile (LC/MS grade) were obtained from Fischer Scientific. Formic acid (LC/MS grade) and kaolinite were purchased from Fluka (Saint-Quentin Fallavier, France). Water (Milli-Q) was purified using a reverse osmosis RIOS 5 and Synergy (Millipore) device (resistivity 18 MΩ cm, DOC < 0.1 mg L^{-1}). All of the products were used as received.

Sample Preparation. The preparation of dry films as a mixture of clay and TCS was performed as follows (26,27,33 and references therein): kaolinite was mixed with a solution of TCS in methanol at a known concentration of 1.0 μmol per 1.0 g of mineral support (unless otherwise specified). The obtained mixture was vigorously stirred in order to obtain a homogeneous dispersion of TCS and the mineral support. Then, a specific volume (that varies with respect to the desired layer thickness) was deposited on a known surface area (roughly 3.6 cm^2) by using a glass or quartz plate. The sample was left to dry for roughly 6 h in a laminar flow cabinet.

The prepared samples were then irradiated horizontally using a Suntest CPS photoreactor (Atlas) equipped with a xenon lamp and a filter that prevents the transmission of wavelengths below 290 nm. The lamp was set at the intensity of 750 W m^{-2}. The temperature of the sample was maintained at roughly 15 °C by maintaining a continuous flow of cold water through the bottom of the photoreactor.

After irradiation, the total amount of the solid sample was added to 5.0 mL of methanol, and the mixture was vigorously stirred for 5 min. The solid and the liquid phases were then separated by centrifugation at 13,500 rpm for 10 min. This procedure ensured the recovery of TCS at a percentage ranging from 70 to 75% for the samples with a concentration within the range 0.1−5.0 μmol g^{-1}. All of the results were an average of at least three individual experiments.

The layer thickness was evaluated by considering the density of mineral kaolinite (1.8 g cm^{-3}) by using the following expression (eq 1):[26,27,33]

$$E = \frac{m}{\rho \times S} \times 10^4 \quad (1)$$

Equation 1: determination of the layer thickness of kaolinite

where E is the layer thickness (μm), ρ is the support density (g cm^{-3}), S is the film surface (cm^2), and m is the used mass of the mineral support (g).

Chromatographic and Spectroscopic Analysis. The reflection diffuse spectra were recorded on a Cary 300 scan (Varian) spectrophotometer equipped with a 9 cm integrating sphere, and their analysis was performed according to the published procedure.[27,33]

The HPLC-UV-MS analyses were performed using a Waters Alliance 2695 instrument equipped with a photodiode array detector. A reversed-phase column distributed by Phenomenex (Kinetex MS C18, 2.6 μm, 100 mm × 2.1 mm) equipped with a precolumn was used at a flow rate of 0.2 mL min^{-1}. The mobile phase was composed of acetonitrile (solvent A) and acidified water (formic acid, 0.1% v/v; pH 2.6) (solvent B). To ensure a better separation, the following gradient program was used: 0−15 min, 5% → 95% A (linear); 15−25 min 95% A, 25−35 min 95% → 5% A (linear). Under these conditions, several generated photoproducts were separated. TCS solutions were injected without any further treatment, and the injection volumes were 10.0 and 40.0 μL for LC/ESI-MS and MS/MS experiments, respectively.

The generated products were identified using a Waters/Micromass LC/Q-TOF (Micromass, Manchester, UK), equipped with an orthogonal geometry Z-spray ion source. The irradiated solution was introduced into the atmospheric pressure ionization source after LC separation and ionized by ESI in the positive mode. Mass calibration was first performed preacquisition (H_3PO_4, 85%), and a single lock-mass correction was used during analyses (Trityrosine, Sigma-Aldrich). Scanning was performed with the *m/z range* 90−600. Elemental compositions were further calculated using MassLynx Elemental Composition software v.4.0 (Micromass, Manchester, UK). Maximum deviation was set to 5 ppm, and C, H, N, O, and S were selected as possible constituents. Five scans were combined before the integration of the different peaks.

The desolvation and ion source block temperatures were set at 250 and 100 °C, respectively. Nitrogen was used as a nebulizer (35 L h^{-1}) as well as desolvation gas (350 L h^{-1}). The voltages found for the probe and ion source components (to produce maximum intensity) were 3 kV for the stainless-steel capillary, 35 V for the sample cone, and 1 V for the extractor cone.

Quantum Yield Calculation. The quantum yield under the Suntest excitation was estimated usingeq 2[27,33]

https://doi.org/10.1021/acsomega.3c03101
ACS Omega 2023, 8, 38916−38925

$$k_p^0 = 2.303 \times \int_\lambda \Phi_i \times I_0(\lambda) \times \varepsilon(\lambda) d\lambda$$

$$\Rightarrow \Phi_i = \frac{k_p^0}{2.303 \times \int_\lambda I_0(\lambda) \times \varepsilon(\lambda) d\lambda} \quad (2)$$

Equation 2: Determination of the photodegradataion rate at the surface of kaolinite

where k_p (min^{-1}) is the photodegradation rate at the surface of the substrate, Φ_i the polychromatic quantum yield of the studied molecule, $I_0(\lambda)$ the total light intensity in photons cm^{-2} s^{-1}, and $\varepsilon(\lambda)$ the molar absorption coefficient. The calculation of the quantum yield was performed within the range of 290−310 nm corresponding to the overlap between the emitted light from the Suntest and the absorption spectrum of TCS at the surface of kaolinite.

Simulation Protocol. The TCS molecules were modeled by using the all-atom Amber force field[34] (Figure 1).

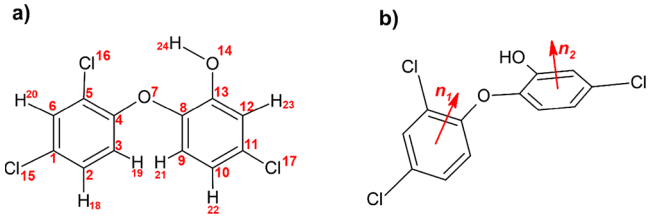

Figure 1. (a) Atomic numbering used in this section. (b) Representation of the normals to the aromatic cycles used to study the conformation of TCS, θ being the (n_1,n_2) angle.

The atomic charges were calculated using the Gaussian package at the B3LYP/6-31g (d,p) level and the ChelpG procedure. The kaolinite crystal was modeled by employing the ClayFF force field.[35] We used the TIP4P/2005 model[36] for water molecules. The molecular dynamics simulations were performed with version 2.20 of the DL_Poly package[34] using a Verlet-Leapfrog algorithm and a time step of 0.5 fs for the integration of forces. This small time step value compared to common values of 1 or 2 fs is imposed by the flexible O−H bonds from the ClayFF force field. The temperature was imposed at T = 298 K using a Nosé−Hoover thermostat with a coupling constant of 0.5 fs. The Lennard-Jones parameters were calculated by Lorentz−Berthelot mixing rules. Periodic boundary conditions were applied to the simulation box along the three directions. The cut-off for short-range interactions was set to 12 Å (van der Waals and real space electrostatics), while the long-range electrostatics were handled using the smooth particle mesh Ewald (SPME) method[37] with a relative error of 10^{-6}.

Each simulation run consisted of a 500 ps equilibration phase followed by a 2 ns production phase during which 8000 configurations were saved (one every 250 fs). Postsimulation analyses were then carried on the saved configuration. The TCS molecule was studied in various environments: solvated in water and in a vacuum and adsorbed on both sides of the kaolinite surface. The simulations of TCS solvated in water were carried out in the constant-NpT ensemble to ensure a correct density of water. The initial box size was 51 × 51 × 51 $Å^3$ containing 4445 water molecules. The vacuum simulations were performed in the constant-NVT ensemble using a 100 × 100 × 100 $Å^3$ bounding box. The adsorbed systems were composed of a kaolinite crystal of size 41.2 × 44.7 × 28.5 $Å^3$ (8 × 5 × 4 unit cells) that is surrounded by a vacuum along the z direction. As a consequence, periodic boundary conditions apply in the x and y directions of the crystal. The z direction of the box is extended with a vacuum of up to 114 Å to avoid interactions along the periodic z axis normal to the surface. The TCS molecules are then placed in a vacuum close to a given face of the kaolinite (gibbsite or siloxane), with a distance of 2 Å between the closest atoms of TCS and kaolinite. The following report reports the variety of systems studied in this work.

a) One TCS molecule in a vacuum.
b) Two close TCS molecules (dimer) in a vacuum.
c) One TCS molecule solvated by water.
d) A TCS dimer solvated in water.
e) One TCS molecule adsorbed onto the gibbsite face of the kaolinite.
f) Several TCS molecules adsorbed onto the gibbsite face of the kaolinite. Depending on the system, the number of TCS molecules is 2, 3, 4, 6, 8, 10, and 12. The TCS molecules were initially located randomly in the xy plane, with only a no overlap criterion.
g) One TCS molecule adsorbed onto the siloxane face of the kaolinite.
h) Several TCS molecules adsorbed onto the siloxane face of the kaolinite. Depending on the system, the number of TCS molecules is 2, 3, 4, 6, 8, 10, and 12. The TCS molecules were initially located randomly in the xy plane with only a no overlap criterion.

RESULTS AND DISCUSSION

Photodegradation of TCS on the Kaolinite Support. In order to have better insight into the spectroscopic features of TCS on kaolinite, we recorded the diffuse-reflection spectrum using an integration sphere at various concentrations (within the range 0.10−5.0 μmol g^{-1}). The reflection diffuse spectrum of TCS at the surface of the kaolinite layer was obtained using the protocol described in the literature and the Kubelka−Munk function[27,33] (Figure SI 1). The absorption maximum was located at 280 nm, and the shape of the spectra was very similar to the results previously reported for the spectra of the neutral form of TCS in aqueous solution.[11] The molar absorption coefficient measured at 280 nm for TCS in kaolinite was found equal to 2.6 × 10^6 mol^{-1} L cm^{-1}, which is lower in comparison to that in aqueous solution (ε_{280} = 4.2 × 10^6 mol^{-1} L cm^{-1}). Such a hypochromic effect can be attributed to the possible chemical and physical interactions between the clay and the organic compound.

When TCS was irradiated at the surface of kaolinite (1.0 μmol g^{-1} of kaolinite with a thickness of 50 μm), an efficient disappearance was observed. The decrease of the concentration of TCS follows a first-order kinetics with an observed rate constant, k_{obs}, evaluated to 3.1 × 10^{-3} min^{-1}. In order to determine the quantum yield of photodegradation of TCS in kaolinite, we studied the photodegradation of TCS in several kaolinite layers of various thicknesses Z. Figure SI 2 indicates that $k_{obs} \times Z$ remains unchanged within the range 20−65 μm. Its value was evaluated to be 1.6 × 10^{-1} μm cm^{-1}. However, such rate constant decreases for higher thickness, indicating that the organic compound diffusion is faster than the photodegradation for samples that are thinner than 65 μm and can therefore be neglected. Under these conditions, using

https://doi.org/10.1021/acsomega.3c03101
ACS Omega 2023, 8, 38916−38925

the same methodology as described by Menager et al.,[26,27] we were able to evaluate the photodegradation rate constant of TCS at the surface of kaolinite to $k_p^0 = 2.9 \times 10^{-4}$ min^{-1} and the quantum yield of photodegradation to $\Phi = 0.90$. This value is considerably higher than the reported quantum yield of photodegradation of TCS in aqueous solution, which is, for example, $\Phi_{aq} = 0.30$ for an irradiation of the neutral form of TCS at 254 nm.[11]

Primary Photoproduct Elucidation and Photodegradation Pathways. Figure 2 represents the HPLC-DAD chromatogram obtained for the irradiation of TCS deposited on kaolinite (1.0 μmol g^{-1} of kaolinite with a thickness of 50 μm) for 180 min in the Suntest apparatus and clearly reveals the formation of several byproducts. Using HPLC/ESI-Q-TOF in negative ion mode, these peaks were associated with seven photoproducts, noted as **P1**, **P2**, **P3**, **P4**, **P5**, **P6**, and **P7** in the order of their retention time. No significant response was obtained in positive ion mode.

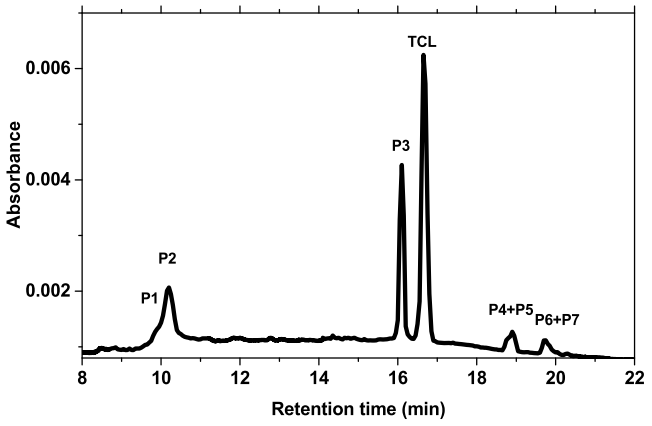

Figure 2. HPLC-DAD chromatogram of irradiated TCS deposited at the surface of kaolinite (1.0 μmol g^{-1} of kaolinite, 50 μm thickness; $\lambda_{detection}$ = 254 nm).

The accurate masses, molecular formulas, and molecular structure of these generated compounds were determined and are presented in Table 1.

Photoproducts **P1** and **P2** were identified as 4-chlorobenzene-1,2-diol and 2,4-dichlorophenol, respectively. These products are the two aromatic moieties of TCS, which suggest that their formation occurs via homolytic cleavage of the C−O etheroxyde bonds of the TCS molecule, followed by a reaction with molecular oxygen. The same primary processes have been described in aqueous solution in our previous study but leading to different photoproducts.[11]

Photoproduct **P3** has been identified as 2,8-dichlorodibenzo-p-dioxine formed via cyclization of TCS. This process has been reported in alkaline aqueous solution where the anionic form of TCS is predominant, involving the triplet excited state of the TCS anion and an intramolecular substitution of a chlorine by the phenolate function. However, the formation of this product has not been observed in an acidic aqueous solution, where the neutral form of TCS is predominant. Since we have deposited the neutral form of TCS on the kaolinite in our experiment, this leads us to the conclusion that the reactivity of TCS is different on the surface of the clay than in aqueous solution.

Photoproducts **P4** and **P5** were attributed the same retention time, but a fine reading of the chromatogram indicated the presence of 2 distinct peaks. Their elemental composition is $C_{24}H_{13}O_4Cl_5$, which suggests that their formation occurs via condensation of 2 TCS molecules, with the loss of a chlorine and a hydrogen atom. The pathway for this condensation is an intermolecular substitution very similar

Table 1. Proposed Structures for the Generated Byproducts P1, P2, P3, P4, P5, P6, and P7, as Obtained by HPLC/MS Analyses

Detected ion	Retention time (min)	Measured mass (*m/z*)	Elemental composition	Error (ppm)	Proposed structure for the neutral compound
[P1–H]$^-$	10.0	142.9898	$C_6H_4O_2Cl^-$	−1.4	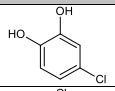
[P2–H]$^-$	10.2	160.9558	$C_6H_3OCl_2^-$	−1.9	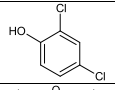
[P3–H]$^-$	16.1	250.9665	$C_{12}H_5O_2Cl_2^-$	−0.8	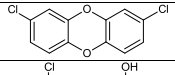
[TCS–H]$^-$	16.6	–	$C_{12}H_6O_2Cl_3^-$	–	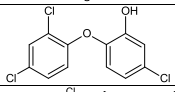
[P4–H]$^-$ [P5–H]$^-$	18.9	538.9171	$C_{24}H_{12}O_4Cl_5^-$	−1.3	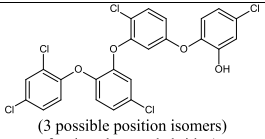 (3 possible position isomers) for the etheroxyde bridge)
[P6–H]$^-$ [P7–H]$^-$	19.9	572.8778	$C_{24}H_{11}O_4Cl_6^-$	−1.3	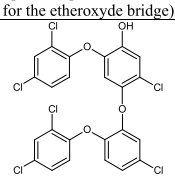 (several possible isomers)

https://doi.org/10.1021/acsomega.3c03101
ACS Omega 2023, 8, 38916−38925

to the intramolecular substitution observed for the formation of photoproduct **P3**. As three chlorine atoms are available on a TCS molecule, 3 position isomers can be formed via this process, each resulting from the substitution of a chlorine to create an etheroxyde bridge between two TCS molecules.

Similar to **P4** and **P5**, photoproducts **P6** and **P7** were attributed to the same retention time but with two distinct peaks. Their elemental composition is $C_{24}H_{12}O_4Cl_6$, suggesting that their formation occurs via condensation of 2 TCS molecules, with the loss of two hydrogen atoms. The pathway for this condensation can be described as the formation of a cation radical formed via photoejection of an electron in the presence of dioxygen, followed by a reaction between the cation radical and another molecule of TCS, as described in the literature in the case of phenol and chlorophenol irradiation.[38,39] Various isomers can be formed by this process, and we could not assign precise structures to **P6** and **P7**.

Effect of TCS Concentration. When the initial concentration of TCS increased from 0.05 to 1.0 μmol g^{-1}, the observed rate constant increased due to the increase of fraction of light absorbed by the molecule up to 3.2×10^{-3} min^{-1}. However, for higher concentrations, we clearly observe a decrease in the rate constant, which reaches 2.6×10^{-3} min^{-1} for a concentration of 2.0 μmol g^{-1}, for example, which is more likely due to a screen effect phenomenon. Moreover, the initial concentration of TCS also had a very strong influence on the nature of the photoproducts formed. Indeed, when the initial concentration of TCS was 5.0 μmol g^{-1}, photoproducts **P4**, **P5**, **P6**, and **P7** (which are all dimers of TCS) appeared as the main photoproducts, whereas **P1** and **P2** were undetected by HPLC-DAD analysis. Figure 3 shows the evolution of the ratio (peak area of **P4** + **P5**/initial peak area of TCS) with the initial concentration of TCS for fixed degradation rates of TCS.

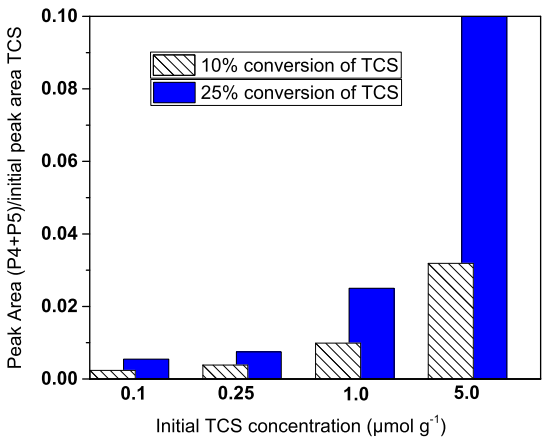

Figure 3. Evolution of the ratio (peak area of **P4** + **P5**/initial peak area of TCS) as a function of the initial concentration of TCS for fixed degradation rates of TCS.

It clearly shows that the formation of **P4** and **P5** is favored at a higher concentration. A similar evolution was obtained in the case of **P6** and **P7**, which indicates that the formation of dimers occurs at a high concentration. No significant influence of the initial concentration of TCS was observed for the formation of photoproduct **P3** at these degradation rates, which is consistent with the fact that it is formed via an intramolecular reaction process. On the contrary, the formations of **P1** and **P2** were favored at lower initial concentrations of TCS, which is consistent with the fact that they are formed via a cleavage process which is a monomolecular process.

Interactions between TCS and Kaolinite Using Molecular Dynamics Simulations. Our previous results showed that both photophysical and photochemical properties of TCS are different in aqueous solution and at the surface of kaolinite. To have better insight into the interaction between TCS in these two media, molecular simulations were used. This was undertaken to simulate and compare the behavior of a single molecule of TCS in 4 different conditions: (1) in vacuum, (2) in pure water, (3) deposited on the siloxane-like surface of a kaolinite crystal, and (4) deposited on the gibbsite-like surface of a kaolinite crystal. Figure 4 represents the snapshots of typical equilibrated configurations of a TCS molecule deposited on each surface of kaolinite.

A first look at the behavior of the molecule during the simulation showed that TCS seemed to have different conformations depending on its environment. In order to confirm this, the distribution of the angle between the two aromatic cycles, θ_{cycle}, was measured as an indicator of the molecule disposition. This angle, named θ_{cycle}, is defined to be equal to zero when both cycles are in the same plane and when the chlorine atom (Cl^{16}) and the phenol function (O^{14}) are both pointing in the same direction as already shown in Figure 1. The distribution of θ_{cycle} during each simulation is presented in Figure 5.

In the case of TCS in a vacuum, the distribution of θ_{cycles} shows a very thin peak centered around 120°, which represents the most stable conformation of TCS. When surrounded by water, the distribution of θ_{cycles} exhibits an additional band centered around 50° in addition to one present in a vacuum, which is much less present. It is interesting to note that the most intense band in water or when deposited on the siloxane-like surface of kaolinite is centered around 50°, which means that the most stable conformation of TCS in this environment is different from its conformation in vacuum. However, when deposited on the gibbsite-like surface of kaolinite, the distribution of θ_{cycles} is more intense around 120°, which means that this conformation is the most stable in this environment. A slight shift is observed in the 50° band depending on the systems as well as in the 120° band compared to that in vacuum. This indicates that the TCS−surface interaction may differ depending on the siloxane/gibbsite face. These results show that the most stable conformation of TCS can be different in water and at the surface of kaolinite, which could explain why the photophysical and photochemical properties of TCS are also different in these two environments.

In order to explain the different conformations of TCS onto the surface, we measured the average number of hydrogen bonds between a TCS molecule and its environment using the following criteria. A hydrogen bond involving 3 atoms O−H··· Y occurs if the distance between H and Y is lower or equal to 2.45 Å, and the $\hat{YOH}$ angle is lower or equal to 30°. The average number was normalized in order to be equal to 1 if at each step of the simulation a hydrogen bond was detected between the environment and studied atoms. This procedure was used for each oxygen atom and chlorine atom of TCS for each simulation, but the only hydrogen bonds detected in significant number (superior to 0.1 in average) involved the phenol function of TCS ($O^{14}H^{24}$), which displayed 0.96 hydrogen bonds in water and 0.98 at the gibbsite-like surface of

https://doi.org/10.1021/acsomega.3c03101
ACS Omega 2023, 8, 38916−38925

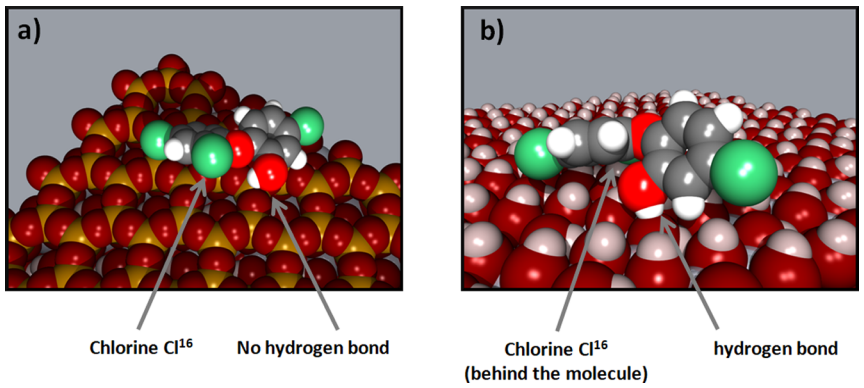

Figure 4. Snapshots of typical equilibrated configurations of a TCS molecule deposited on the siloxane-like surface (a) and the gibbsite-like surface (b) of kaolinite.

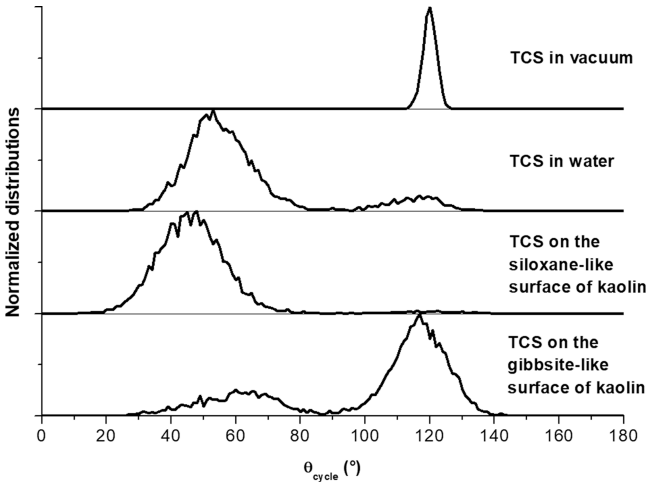

Figure 5. Normalized distribution of the angle between the aromatic cycles θ_{cycle} for the simulation of a TCS molecule in various environment.

kaolinite. This results show that TCS is very strongly bonded to the gibbsite-like surface of kaolinite via this interaction. In the case of TCS deposited on the siloxane-like surface, no significant hydrogen bond was detected (average number of 0.09) owing to the absence of hydroxyl groups at the surface. We conclude that in the case of water and the gibbsite-like surface of kaolinite, the phenol function of TCS aligns with the nearby oxygen atoms in order to establish hydrogen bonds, either with water molecules or with the hydroxyl groups of the surface. This specific geometry was not observed in the case of the siloxane-like surface, which does not possess hydroxyl groups.

In the case of TCS deposited on both the siloxane-like surface and gibbsite-like surface of kaolinite, the atomic density for the atoms of TCS along the z axis was measured as an indicator of the adsorption of TCS on the surface and is represented in Figure 6.

In the case of the siloxane-like surface, the atomic density is shaped as a wide peak ranging from 0.5 to 7.5 Å, with a maximum at 2.2 Å, whereas in the case of the gibbsite-like

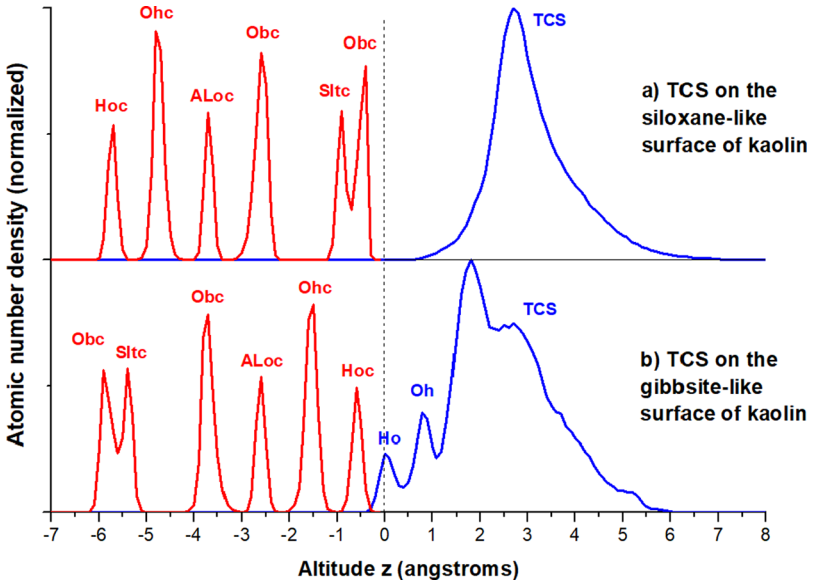

Figure 6. Atomic number density along the z axis for the simulation of a TCS molecule deposited on the siloxane-like surface (a) and the gibbsite-like surface (b) of kaolinite. The origin of the z axis was placed at the altitude of the highest atom of kaolinite. Density profiles for kaolinite atoms (in red) and TCS atoms (in blue) have been calculated and normalized separately (Obc: bridging O; ohc: O of hydroxyl group; Hoc: H of hydroxyl group; ALoc; octahedral Al; SItc: octahedra Si; Ho: H of hydroxyl group of TCS; Oh: O of hydroxyl group of TCS).

https://doi.org/10.1021/acsomega.3c03101
ACS Omega 2023, 8, 38916−38925

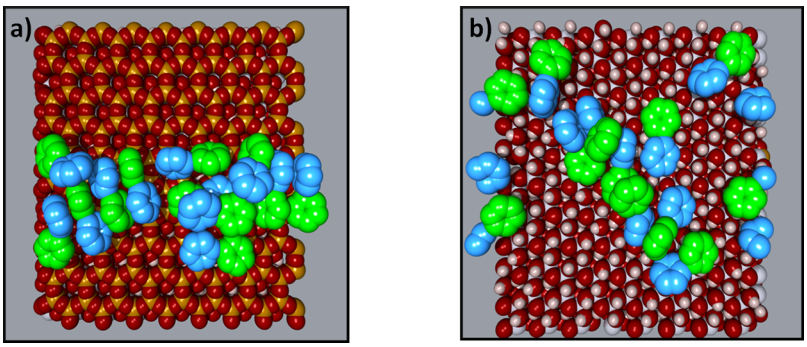

Figure 7. Snapshots of typical equilibrated configurations of 12 TCS molecules deposited on the siloxane-like surface (a) and the gibbsite-like surface (b) of kaolinite.

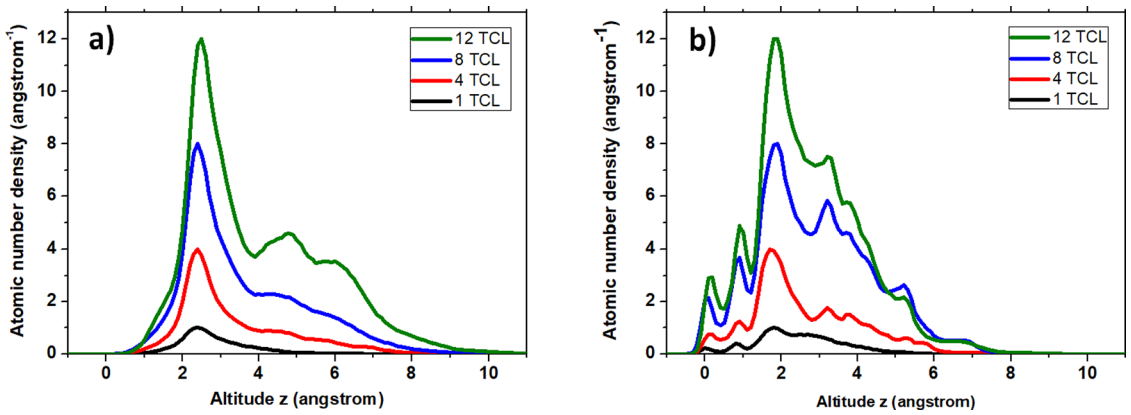

Figure 8. Atomic number density along the z axis for the simulation of 1, 4, 8, and 12 TCS molecules deposited on the siloxane-like surface (a) and the gibbsite-like surface (b) of kaolinite. The origin of the z axis was placed at the altitude of the highest atom of kaolinite.

surface, it shows 4 peaks (0; 0.8; 1,8; and 2.7 Å) and ranges from −0.4 to 6.0 Å. Stronger structuring and smaller values of the atomic density mean that the adsorption of TCS on the gibbsite-like surface is stronger and more rigid than on the siloxane-like surface. Moreover, the peaks observed at 0 and 0.8 Å can be attributed to the atoms O^{14} and H^{24}, which are involved in the hydrogen bond with the hydroxyl groups on the gibbsite-like surface.

These results show that studying both surfaces is justified to understand the adsorption of TCS since a real kaolinite surface can be admitted as an intermediate between a siloxane surface and a gibbsite surface, which have very different interactions with the TCS molecule.

Cluster formation at the surface of Kaolinite: The formation of photoproducts **P4**, **P5**, **P6**, and **P7**, which are the results of TCS dimerization during the irradiation at the concentration of 1.0 μmol g^{-1} or higher, suggests that the molecules of TCS are close to each other at the surface of kaolinite. However, at this concentration, a quick calculation can show us that less than 2% of the kaolinite surface is covered by the TCS molecules (for this calculation, we have estimated that the surface covered by one TCS molecule is lower than 50 $Å^2$ and that the specific surface of kaolinite used is 14.5 m^2 g^{-1}) as reported in the literature.[11] This suggests that the repartition of the TCS molecules at the surface of the clay is not homogeneous but that the molecules join each other to form clusters. In order to validate this idea and have a better understanding of the structure and stability of the supposed clusters, molecular dynamics was used to simulate the behavior of 4, 8, or 12 TCS molecules deposited close to each other at the surface of a kaolinite crystal. The simulations were performed either on a gibbsite-like surface or on a siloxane-like surface to compare these two different environments available at the surface of the clay. The $\pi-\pi$ interaction between the aromatic systems of two or more TCS molecules is the most probable driving force for the creation of clusters. Despite the fact that the Amber force field does not explicitly model the π-staking interactions, the parameterization of the aromatic carbon is supposed to create such structures as it is energetically favorable. As a consequence, we aim at quantifying the amount of π-stacking by using geometric criteria based on the angles between the normal and aromatic cycles belonging to the two TCS molecules close to each other. Supporting Information (Figures SI 3 and SI 4) shows the results obtained for the interactions between two molecules of TCS and the geometric criteria selection for the detection of π-stacking interactions between two aromatic cycles.

Figure 7 gives snapshots of the final configurations of the simulation of 12 TCS molecules deposited close to each other on a siloxane-like surface and on a gibbsite-like surface of kaolinite. In order to better visualize the orientation of the molecules and the π-stacking interactions, only carbon atoms have been represented and aromatic cycles have been colored in blue (for the cycle holding the hydroxyl group) and in green.

A first look at the behavior of the molecule during the simulation showed that the TCS molecules stay very close to each other and that a compact cluster is formed in both the surfaces with a higher density of the cluster on the siloxane-like surface than on the gibbsite-like one. Moreover, several molecules are overlapping, which causes some aromatic cycles

https://doi.org/10.1021/acsomega.3c03101
ACS Omega 2023, 8, 38916−38925

to be apart from the clay surface. In order to confirm this observation, atomic number density along the z axis was measured for each simulation as presented in Figure 8.

In the case of the siloxane-like surface, the atomic number density extends beyond 6 Å when 4 molecules of TCS were deposited on the surface and even beyond 8 Å in the case of 12 TCS, which clearly indicates that some molecules are overlapping and separating from the surface due to the formation of a dense cluster. In the case of the gibbsite-like surface, the thin peaks at 0 and 0.8 Å suggest that the hydrogen bond between the phenol group of TCS and the surface that was observed in the simulation of a single TCS molecule is preserved even with a higher number of TCS molecules. It was confirmed by the measurement of the average number of hydrogen bonds per TCS molecule, which ranged from 0.9 to 1.0 in each of the simulations on this surface. On this surface, the atomic number density becomes very low above 6 Å, which indicates that the overlapping is less likely to occur, which can be explained by the fact that the molecules are strongly anchored to the surface via the hydrogen bond and therefore have less available conformations. However, this does not mean that the molecule cannot aggregate into a cluster since they still have enough liberty to align and interact with each other.

In order to measure the interaction between the TCS molecules, the average number of π-stacking interactions per aromatic cycle, N_π, has been measured for each simulation (Table 2). The criteria for the detection of π-stacking interactions and the calculation of N_π have been chosen after the simulation of a stable dimer of TCS in a vacuum, where the aromatic cycles of the two molecules remained parallel and close to each other during the whole simulation (this simulation and its results are discussed in detail in the Supporting Information).

Table 2. Average Number of π-Stacking Interactions N_π in the Simulations of Several TCS Molecules on the Siloxane-like Surface and the Gibbsite-like Surface of Kaolinite

number of TCS molecules	4	8	12
N_π on the siloxane-like surface	0.44	0.50	0.73
N_π on the gibbsite-like surface	0.55	0.52	0.51

For each simulation, the value of N_π is close to 0.5 or above, which was the value obtained for the stable dimer of TCS simulated in vacuum. This shows that the molecules of TCS are strongly associated with each other via π-stacking interactions and confirms the formation of a cluster on both the surfaces. Moreover, in the case of the siloxane-like surface of kaolinite, a very high value of 0.73 is obtained for the simulation of 12 TCS, which is consistent with the significant overlap previously observed. In the case of the gibbsite-like structure, the stable value of N_π around 0.5 shows that, even if the molecules are firmly bonded to the surface via chemisorption, they can aggregate into a cluster and strongly interact with each other.

These results clearly demonstrate that the formation of a stable cluster is possible on a real kaolinite surface, which can be thought of as an intermediate between a siloxane and a gibbsite surface and is governed by the π-stacking interactions between the aromatic moieties of TCS molecules. The hydrogen bonds with the surface prevent the molecule from overlapping but do not prevent the π-stacking intermolecular interactions.

CONCLUSIONS

The photodegradation of TCS at the surface of kaolinite was deeply examined. The disappearance quantum yield was evaluated to 0.90 that is considerably higher than that obtained in aqueous solution indicating a specific photochemical behavior on such support. This aspect was further confirmed by the elucidation of the photogenerated byproducts. In particular, the formation of dioxin derivatives occurs with a relatively high yield. Moreover, when TCS was used at high concentrations (>1.0 μmol g^{-1}), the formation of dimer-type photoproducts was clearly favored. These findings clearly demonstrate that specific interactions with kaolinite are involved. Such interactions were deeply studied using molecular dynamic modeling. TCS appears to be effectively linked to the surface of kaolinite by hydrogen bonds involving the phenolic moiety conferring to the system a specific conformation. Moreover, at the surface of such a solid support, several TCS molecules interact together through the π-staking process giving rise to the formation of clusters that may lead to the formation of dimer-type byproducts.

ASSOCIATED CONTENT

Supporting Information

The Supporting Information is available free of charge at https://pubs.acs.org/doi/10.1021/acsomega.3c03101.

Comparison of the absorption spectrum of TCS in aqueous solution and at the surface of kaolinite as obtained by reflection diffuse spectroscopy, effect of the kaolinite thickness on the photodegradation rate constant of TCS, and study of the interactions between two molecules of TCS and definition of the geometric criteria for the detection of π-stacking interactions between two aromatic cycles (PDF)

AUTHOR INFORMATION

Corresponding Author

Mohamed Sarakha − *CNRS, Clermont Auvergne INP, ICCF, Université Clermont Auvergne, F-63000 Clermont-Ferrand, France;* orcid.org/0000-0002-7508-3387; Phone: 00 33 4 73 40 71 71; Email: mohamed.sarakha@uca.fr

Authors

Cyril Le Fur − *CNRS, Clermont Auvergne INP, ICCF, Université Clermont Auvergne, F-63000 Clermont-Ferrand, France*

Florent Goujon − *CNRS, Clermont Auvergne INP, ICCF, Université Clermont Auvergne, F-63000 Clermont-Ferrand, France;* orcid.org/0000-0001-7511-3905

Pascal Wong Wah Chung − *CNRS, LCE, UMR, Aix Marseille Univ, 7376 Marseille, France*

Patrice Malfreyt − *CNRS, Clermont Auvergne INP, ICCF, Université Clermont Auvergne, F-63000 Clermont-Ferrand, France;* orcid.org/0000-0002-3710-5418

Complete contact information is available at: https://pubs.acs.org/10.1021/acsomega.3c03101

Notes

The authors declare no competing financial interest.

https://doi.org/10.1021/acsomega.3c03101
ACS Omega 2023, 8, 38916−38925

■ ACKNOWLEDGMENTS

The authors wish to thank the *Université Clermont Auvergne* for financial support (PhD scholarship of C.L.F.).

■ REFERENCES

(1) McMurry, L. M.; Oethinger, M.; Levy, S. B. Triclosan Targets Lipid Synthesis. *Nature* **1998**, *394*, 531−532.
(2) Yazdankhah, S. P.; Scheie, A. A.; Hoiby, E. A.; Lunestad, B. T.; Heir, E.; Fotland, T.-O.; Naterstad, K.; Kruse, H. Triclosan and antimicrobial resistance in bacteria: an overview. *Microb. Drug Resist.* **2006**, *12* (2), 83−90.
(3) Olaniyan, L. W. B.; Mkwetshana, N.; Okoh, A. I. Triclosan in water, implications for human and environmental health. *SpringerPlus* **2016**, *5*, 1639 DOI: 10.1186/s40064-016-3287-x.
(4) Foran, C. M.; Bennett, E. R.; Benson, W. H. Developmental evaluation of a potential non-steroidal estrogen: triclosan. *Mar. Environ. Res.* **2000**, *50*, 153−156.
(5) Halden, R. U. On the Need and Speed of Regulating Triclosan and Triclocarban in the United States. *Environ. Sci. Technol.* **2014**, *48*, 3603−3611.
(6) Chuanchuen, R.; Beinlich, K.; Hoang, T. T.; Becher, A.; Karkhoff-Schweizer, R. R.; Schweizer, H. P. Cross-Resistance between Triclosan and Antibiotics in *Pseudomonas aeruginosa* Is Mediated by Multidrug Efflux Pumps: Exposure of a Susceptible Mutant Strain to Triclosan Selects *nfxB* Mutants Overexpressing MexCD-OprJ. *Antimicrob. Agents Chemother.* **2001**, *45* (2), 428−432.
(7) Wang, Y.; Song, J.; Wang, X.; Qian, Q.; Wang, H. Study on the toxic-mechanism of triclosan chronic exposure to zebrafish (Danio rerio) based on gut-brain axis. *Sci. Total Environ.* **2022**, *844*, No. 156936, DOI: 10.1016/j.scitotenv.2022.156936.
(8) Geens, T.; Roosens, L.; Neels, H.; Covaci, A. Assessment of human exposure to bisphenol-A, triclosan and tetrabromobisphenol-A through indoor dust intake in Belgium. *Chemosphere* **2009**, *76* (6), 755−760.
(9) Adolfsson-Erici, M.; Petterson, M.; Parkkonen, J.; Sturve, J. Triclosan, a commonly used bactericide found in human milk and in the aquatic environment in Sweden. *Chemosphere* **2002**, *46*, 1485−1489.
(10) Rüdel, H.; Böhmer, W.; Müller, M.; Fliedner, A.; Ricking, M.; Teubner, D.; SchröterKermani, C. Retrospective study of triclosan and methyl-triclosan residues in fish and suspended particulate matter: results from the German Environmental Specimen Bank. *Chemosphere* **2013**, *91* (11), 1517−1524.
(11) Wong-Wah-Chung, P.; Rafqah, S.; Voyard, G.; Sarakha, M. Photochemical behaviour of triclosan in aqueous solutions: Kinetic and analytical studies. *J. Photochem. Photobiol. A Chem.* **2007**, *191* (2−3), 201−208.
(12) Mezcua, M.; Gomez, M. J.; Ferrer, I.; Agüera, A.; Hernando, M. D.; Fernandez-Alba, A. Evidence of 2,7/2,8-dibenzodichloro-p-dioxin as a photodegradation product of triclosan in water and wastewater samples. *Anal. Chim. Acta* **2004**, *524*, 241−247.
(13) Tixier, C.; Singer, H. P.; Canonica, S.; Müller, S. R. Phototransformation of Triclosan in Surface Waters: A Relevant Elimination Process for This Widely Used Biocide Laboratory Studies, Field Measurements, and Modeling. *Environ. Sci. Technol.* **2002**, *36*, 3482−3489.
(14) Latch, D. E.; Packer, J. L.; Stender, B. L.; Vanoverbeke, J.; Arnold, W. A.; McNeill, K. Aqueous photochemistry of triclosan: formation of 2,4-dichlorophenol, 2,8-dichlorodibenzo-p-dioxin, and oligomerization products. *Environ. Toxicol. Chem.* **2005**, *24*, 517−525.
(15) Buth, J. M.; Grandbois, M.; Vikesland, P. J.; McNeill, K.; Arnold, W. A. Aquatic photochemistry of chlorinated triclosan derivatives: potential source of polychlorodibenzo-p-dioxins. *Environ. Toxicol. Chem.* **2009**, *28* (12), 2555−2563.
(16) Apell, J. N.; Kliegman, S.; Sola-Gutiérrez, C.; McNeill, K. Linking Triclosan's Structural Features to Its Environmental Fate and Photoproducts. *Environ. Sci. Technol.* **2020**, *54*, 14432−14441.
(17) Wu, C.; Spongberg, A. L.; Witter, J. D. Adsorption and degradation of triclosan and triclocarban in soils and biosolids-amended soils. *J. Agric. Food Chem.* **2009**, *57* (11), 4900−4905.
(18) Armstrong, L.; Lozano, N.; Rice, C. P.; Ramirez, M.; Torrents, A. Degradation of triclosan and triclocarban and formation of transformation products in activated sludge using benchtop bioreactors. *Environ. Res.* **2018**, *161*, 17−25.
(19) Healy, M. G.; Fenton, O.; Cormican, M.; Peyton, D. P.; Ordsmith, N.; Kimber, K.; Morrison, L. Antimicrobial compounds (triclosan and triclocarban) in sewage sludges, and their presence in runoff following land application. *Ecotoxicol. Environ. Saf.* **2017**, *142*, 448−453.
(20) Butler, E.; Whelan, M. J.; Sakrabani, R.; van Egmond, R. Fate of triclosan in field soils receiving sewage sludge. *Environ. Pollut.* **2012**, *167*, 101−109.
(21) Svenningsen, H.; Henriksen, T.; Priemé, A.; Johnsen, A. R. Triclosan affects the microbial community in simulated sewage-drain-field soil and slows down xenobiotic degradation. *Environ. Pollut.* **2011**, *159* (6), 1599−1605.
(22) Latch, D. E.; Packer, J. L.; Arnold, W.; McNeill, K. Photochemical conversion of triclosan to 2,8-dichlorodibenzo-p-dioxin in aqueous solution. *J. Photochem. Photobiol. A Chem.* **2003**, *158* (1), 63−66.
(23) Aranami, K.; Readman, J. W. Photolytic degradation of triclosan in freshwater and seawater. *Chemosphere* **2007**, *66* (6), 1052−1056.
(24) Sanchez-Prado, L.; Llompart, M.; Lores, M.; García-Jares, C.; Bayona, J. M.; Cela, R. Monitoring the photochemical degradation of triclosan in wastewater by UV light and sunlight using solid-phase microextraction. *Chemosphere* **2006**, *65* (8), 1338−1347.
(25) Mezcua, M.; Gómez, M. J.; Ferrer, I.; Aguera, A.; Hernando, M. D.; Fernández-Alba, A. R. Evidence of 2,7/2,8-dibenzodichloro-p-dioxin as a photodegradation product of triclosan in water and wastewater samples. *Anal. Chim. Acta* **2004**, *524*, 241−247.
(26) Menager, M.; Siampiringue, M.; Sarakha, M. Photochemical behaviour of phenylbenzoquinone at the surface of the clays: Kaolinite, bentonite and montmorillonite. *J. Photochem. Photobiol. A Chem.* **2009**, *208* (2−3), 159−163.
(27) Menager, M.; Sarakha, M. Simulated solar light photo-transformation of organophosphorus azinphos methyl at the surface of clays and goethite. *Environ. Sci. Technol.* **2013**, *47* (2), 765−772.
(28) Buth, J. M.; Steen, P. O.; Sueper, C.; Blumentritt, D.; Vikesland, P. J.; Arnold, W. A.; McNeill, K. Dioxin photoproducts of triclosan and its chlorinated derivatives in sediment cores. *Environ. Sci. Technol.* **2010**, *44* (12), 4545−4551.
(29) Gieguzynska, E.; Amine-Khodja, A.; Trubetskoj, O. A.; Trubetskaya, O. E.; Guyot, G.; ter Halle, A.; Golebiowska, D.; Richard, C. Compositional differences between soil humic acids extracted by various methods as evidenced by photosensitizing and electrophoretic properties. *Chemosphere* **2009**, *75* (8), 1082−1088.
(30) Cawley, K. M.; Hakala, J. A.; Chin, Y.-P. Evaluating the triplet state photoreactivity of dissolved organic matter isolated by chromatography and ultrafiltration using an alkylphenol probe molecule. *Limnol. Oceanogr.: Methods* **2009**, *7*, 391−398.
(31) Frimmel, F. H. Photochemical aspects related to humic substances. *Environ. Int.* **1994**, *20* (3), 373−385.
(32) Katagi, T. Photoinduced oxidation of the organophosphorus fungicide tolclofos-methyl on clay minerals. *J. Agric. Food Chem.* **1990**, *38*, 1595−1600.
(33) Balmer, M. E.; Goss, K. U.; Schwarzenbach, R. Photolytic transformation of organic pollutants on soil surface - An experimental approach. *Environ. Sci. Technol.* **2000**, *34* (7), 1240−1245.
(34) Wang, J.; Wolf, R. M.; Caldwell, J. W.; Kollman, P. A.; Case, D. A. Development and Testing of a General AMBER Force Field. *J. Comput. Chem.* **2004**, *25*, 1157−1174.
(35) Cygan, R. T.; Liang, J.-J.; Kalinichev, G. Molecular Models of Hydroxide, Oxyhydroxide, and Clay Phases and the Development of a General Force Field. *J. Phys. Chem. B* **2004**, *108*, 1255−1266.

https://doi.org/10.1021/acsomega.3c03101
ACS Omega 2023, 8, 38916−38925

(36) McBride, C.; Vega, C.; Noya, E. G.; Ramïrez, R.; Sesé, L. M. Quantum contributions in the ice phases: The path to a new empirical model for water - TIP4PQ/2005. *J. Chem. Phys.* **2009**, *131*, No. 024506.
(37) Essmann, U.; Perera, L.; Berkowitz, M. L.; Darden, T.; Lee, H.; Pedersen, L. G. A smooth particle mesh Ewald method. *J. Chem. Phys.* **1995**, *101*, 8577 DOI: 10.1063/1.470117.
(38) Coulangeon, L.-M.; Perbet, G.; Boule, P.; Lemaire, J. Processus primaire de la photolyse et de la photo-oxydation de l'o-phenyl-phenol. *Can. J. Chem.* **1980**, *58*, 2230−2235.
(39) Oudjehani, K.; Boule, P. Photoreactivity of 4-chlorophenol in aqueous solutions. *J. Photochem. Photobiol. A Chem.* **1992**, *68*, 363−373.

https://doi.org/10.1021/acsomega.3c03101
ACS Omega 2023, 8, 38916−38925